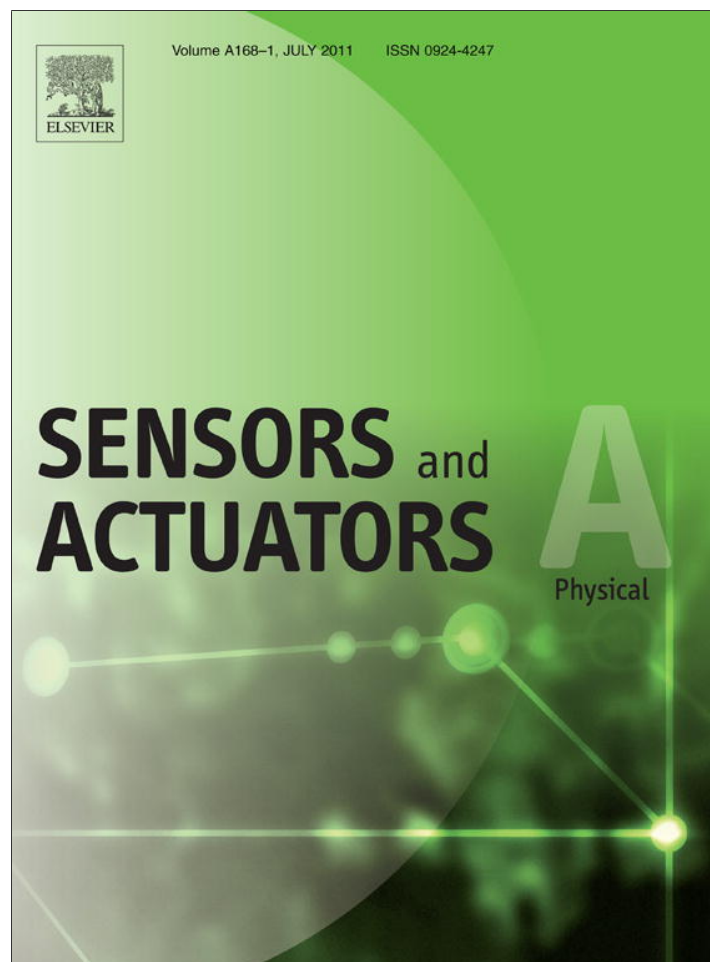


Provided for non-commercial research and education use.
Not for reproduction, distribution or commercial use.



This article appeared in a journal published by Elsevier. The attached copy is furnished to the author for internal non-commercial research and education use, including for instruction at the authors institution and sharing with colleagues.

Other uses, including reproduction and distribution, or selling or licensing copies, or posting to personal, institutional or third party websites are prohibited.

In most cases authors are permitted to post their version of the article (e.g. in Word or Tex form) to their personal website or institutional repository. Authors requiring further information regarding Elsevier's archiving and manuscript policies are encouraged to visit:

<http://www.elsevier.com/copyright>



Contents lists available at ScienceDirect

Sensors and Actuators A: Physical

journal homepage: www.elsevier.com/locate/sna

A novel fabrication of ionic polymer–metal composite membrane actuator capable of 3-dimensional kinematic motions

Zheng Chen*, Tae I. Um, Hilary Bart-Smith

Bio-inspired Engineering Research Lab, Department of Mechanical & Aerospace Engineering, University of Virginia, Charlottesville, VA 22904, USA

ARTICLE INFO

Article history:

Received 16 November 2010

Accepted 2 February 2011

Available online 5 March 2011

Keywords:

Ionic polymer–metal composites

Biomimetic actuation

Bio-inspired robot

ABSTRACT

Ionic polymer–metal composites (IPMCs) are one type of wet electroactive polymers that show promising actuating properties in many bio-inspired underwater robotic applications. In these applications, 3-dimensional kinematic motions are desirable to generate high efficient thrust and maneuverability. However, traditional IPMCs are limited in being only able to generate bending motion. In this paper, a novel synthesis technique is developed to fabricate a hybrid IPMC membrane actuator capable of generating 3-dimensional (3D) kinematic motions. The actuator consists of separated IPMC beams bonded with a soft polydimethylsiloxane (PDMS) membrane. By controlling each individual IPMC beams, we can generate complex 3D motions such as oscillation and undulation. IPMC beams are cut from one sheet of IPMC, which is fabricated through chemically plating platinum electrodes on a Nafion film. A multiple plating process is used to enhance the conductivity of the electrodes, which leads to better actuation performance of IPMC. An assembly based fabrication process is adopted to bond the IPMC actuators with PDMS gel using two CNC-machined molds. Then the PDMS is cured at room temperature to form an actuating membrane. Overall this novel synthesis technique is cost effective and less time-consuming compared to existing strategies. The characterization of the actuating membrane has shown that the maximum twist angle can reach up to 15°, the flapping deflection can reach up to 25% of spanwise length, the tip force can reach up to 0.5 g force, and the power consumption is below 0.5 W. The first application of this novel membrane actuator is in the design of a free-swimming robotic batoid ray. The robot consists of two membranes functioning as artificial pectoral fins. Experimental results show that the robot is capable of free swimming with low power consumption.

© 2011 Elsevier B.V. All rights reserved.

1. Introduction

Electroactive polymers (EAP), sometimes referred to as artificial muscles, are able to generate large deflections under electrical stimuli [1]. Ionic polymer metal composites (IPMCs) are a well-known type of EAP [2]. An IPMC consists of one ion exchange membrane, such as Nafion, coated with two thin metal electrodes [3]. When hydrated, the positive ions (such as sodium or calcium ions) in the Nafion film can move freely, whereas the negative ions are fixed in position due to the bond with the carbon chain in the polymer. Application of an electric field causes the hydrated cations to move to the cathode side while the negative ions are fixed in position. This ion movement introduces swelling in the cathode side and shrinking in the anode side, which leads to a bending motion. Fig. 1 illustrates the actuation mechanism of IPMC.

Since IPMCs can work well in a water environment, they have shown promise as actuators in bio-inspired underwater robots. For example, researchers have used IPMC actuators in the design of an artificial caudal fin [4–8]. This propulsive fin mimics the bending motion observed in many fish species. However, in some other species such as the manta ray (shown in Fig. 2), 3-dimensional kinematic motions are necessary to generate high efficient propulsion and maneuvering [9]. Other applications where complex deformations are desirable include contour control of space inflatable structures [10] and tunable mirror membranes [11]. In order to achieve complex 3D kinematics, Riddle, et al. [12] developed masking and surface machining techniques to pattern the electrodes in IPMC actuators. However, the twist motion was limited by the relatively stiff and non-stretchable Nafion in the passive area. Chen and Tan [13] applied lithographic patterning technology to design an artificial pectoral fin. They modulated the stiffness of the passive area by etching down the Nafion with plasma. This fabrication process has proven to be good for fabricating fins with micron scale features. However, the process involves lithography patterning, plasma etching, and PVD deposition, all which are expensive and time consuming. Additionally, controlling the compliance

* Corresponding author. Tel.: +1 517 6146202; fax: +1 432 9822037.

E-mail addresses: zc7u@virginia.edu (Z. Chen), tiu2f@virginia.edu (T.I. Um), hb8h@virginia.edu (H. Bart-Smith).

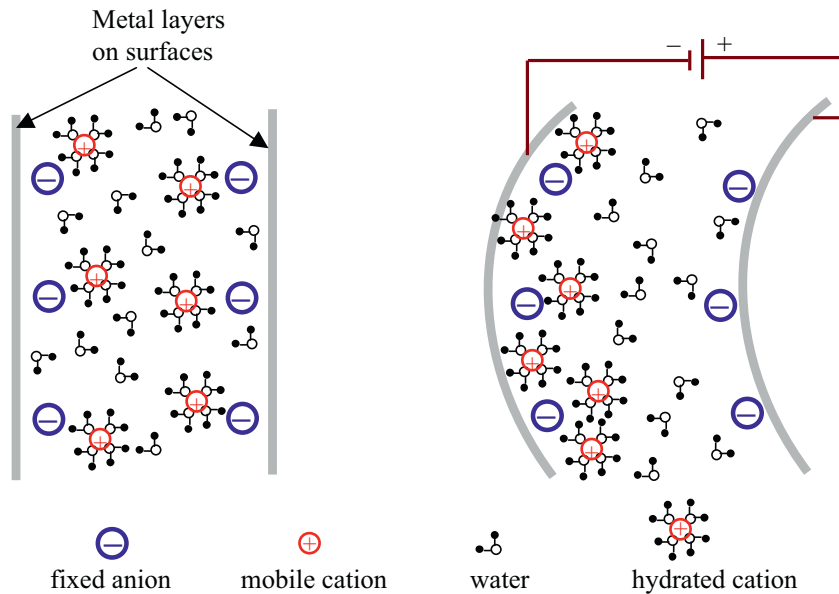


Fig. 1. Actuation mechanism of IPMC (Cross-section view) [2].

characteristics of the passive area is severely limited. Anton et al. [14] developed pectoral fins for a robotic manta ray by assembling separated IPMC beams with latex foil. However, the bonding between IPMCs and latex foil was not seamless, which detrimentally impacted the propulsive efficiency of the fin. Consequently, the robot consumed a large amount of power and required a stack of heavy car batteries for operation, which limited its free-swimming capabilities.

In this study, we have developed a novel synthesis technique to fabricate a soft, lightweight, seamless, and active IPMC membrane actuator capable of creating 3D kinematic motions. The membrane actuator consists of several IPMC beams seamlessly bonded with a soft and stretchable polydimethylsiloxane (PDMS) membrane. Each IPMC beam is controlled individually to produce bending motions of different amplitude and phase, leading to complex kinematic motions. IPMC beams are cut from an IPMC sheet that is fabricated through ion exchange and electroless platinum plating of a Nafion film. The IPMC beams are positioned and clamped between two plastic molds that have been fabricated using CNC milling machine. PDMS gel is poured into the gap between the molds and the whole membrane is cured at room temperature. When the molds are removed, we are left with an IPMC membrane actuator capable

of complex 3D deformation. This fabrication technique offers two major advantages compared to the existing techniques: (1) selection of PDMS elastomer allows for a very compliant passive area; (2) creation of a seamless bond between the IPMC active area and PDMS passive membrane. The actuating membrane is characterized in terms of tip deflection, tip blocking force, twist angle, and power consumption which are the key factors in the design of the bio-inspired robot. Multiple laser sensors are used to characterize the complex deformation on the membrane.

To demonstrate the capabilities of this new type of actuator design, a small size robotic manta ray has been successfully built and tested. This robot has two artificial pectoral fins that are fabricated using this novel technique. Each fin consists of four IPMC strips with a 190 μm thick PDMS membrane. The overall shape of the fin mimics that of biology. A lightweight and compact on-board control unit, with a PCB board and a lithium ion polymer battery, has been built, which enables the robot to swimming freely. This is the first demonstration of a free swimming robotic manta ray propelled by IPMC artificial muscles. Since the pectoral fin can easily be fabricated in different shapes and dimensions, this research provides a platform to investigate the propulsion mechanism of different types of rays.

The rest of this paper is organized in the following manner. Artificial pectoral fin fabrication is described in Section 2. Charac-



Fig. 2. Bio-inspiration: manta ray (courtesy of www.elasmodiver.com).

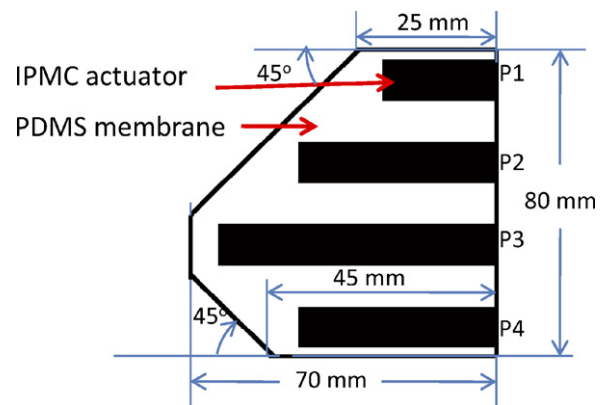


Fig. 3. Design of the IPMC membrane actuator.

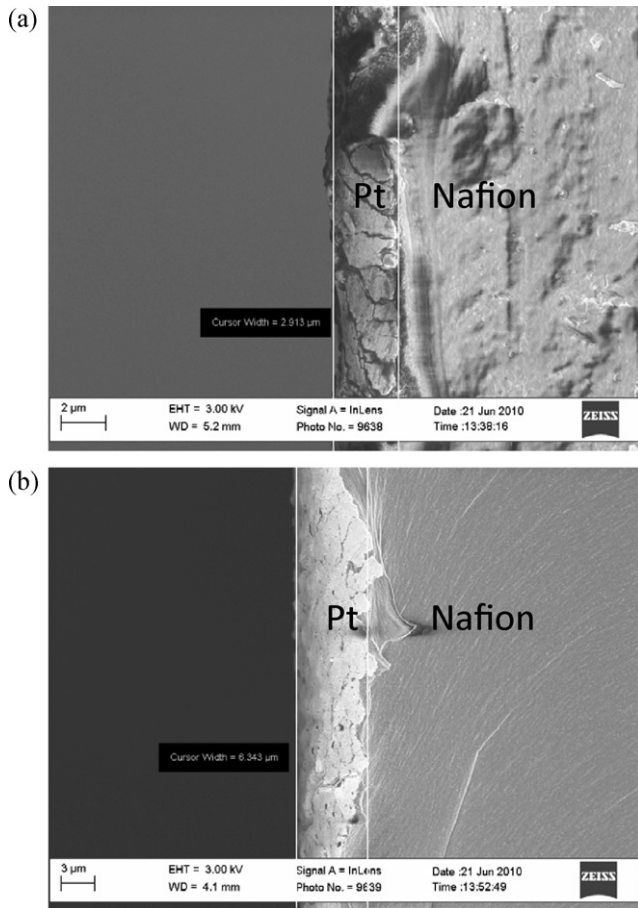


Fig. 4. SEM picture of the platinum electrode in IPMC (cross-sectional view). (a) With one platinum deposition; (b) with two platinum depositions.

terization of the pectoral fin is discussed in Section 3. Application to a robotic manta ray is shown in Section 4 where design and free swimming testing results are presented. Conclusion and future work are discussed in Section 5.

2. Fabrication process

The IPMC membrane actuator is fabricated by assembling IPMC actuators with a PDMS elastomer template to create a predefined planform shape. By controlling the IPMC actuators individually, the membrane is able to generate complex 3D kinematic motions. The

design of the membrane actuator is shown in Fig. 3 where P1, P2, P3, and P4 are 1 cm wide IPMC beams with 3 cm, 5 cm, 7 cm, and 5 cm lengths, respectively.

2.1. Fabrication of IPMC

A new fabrication technique has been developed to create an IPMC-based actuating membrane, capable of complex 3D deformations. The first step in the process is to synthesize the IPMC actuator. Many groups have developed different IPMC fabrication processes to accommodate various functions [2,15–17]. In this current study, we follow most of the fabrication procedure outlined in [15] but add a multiple platinum plating process that reduces the surface resistance of the electrodes to improve the actuation performance [18]. The following supplies are used to fabricate the IPMC beams: (1) Nafion ion exchange membrane Nafion 1110 (258 μm thick, DuPont); (2) tetraammineplatinum chloride 98% (Aldrich); (3) sodium borohydride (NaBH₄, Aldrich); (4) dilute ammonium hydroxide solution (NH₄OH 29% solution); (5) dilute hydrochloric acid (HCl aq, 1.0 N solution); (6) de-ionized water. The major fabrication steps are as follows:

Step 1 Treatment of Nafion with HCl (cleaning). This step is to remove metal particles and other impurities from the film. The Nafion film (10 cm by 5 cm) is boiled in 1.0 N hydrochloric acid (HCl) at 80° for 30 min. The film is then rinsed with DI water to remove acid residue.

Step 2 Ion exchange process: the purpose of the ion exchange process is to enable the Nafion film to absorb enough platinum complex ions Pt(NH₄)₂⁺², which will be reduced to platinum particles to form electrodes in step 3. The membrane is then immersed in 50 ml tetraammineplatinum Chloride hydrate solution (3 mg/ml) mixed with 1 ml ammonium hydroxide (29%) to make a weak base environment. The ion exchange process takes about 3 h to allow the Nafion film to fully absorb enough platinum complex ions.

Step 3 Electroless platinum plating. In this step, the platinum complex ions are reduced to platinum particles to create the metal electrodes on the outer surfaces of the Nafion film. The ion-exchanged Nafion film is placed in a DI water bath. Then the bath is gradually heated to 40 °C. A sodium boron hydride solution (NaBH₄) (20 mg/ml) is prepared, which is used as a reducing agent. 5 ml NaBH₄ solution is added to the bath and the temperature of the bath is increased to 65 °C. 5 ml NaBH₄ solution is added to the bath every 30 min. After 3 h plating, about 3 μm platinum electrode is deposited on the surface. Then the IPMC is rinsed with DI water. An SEM

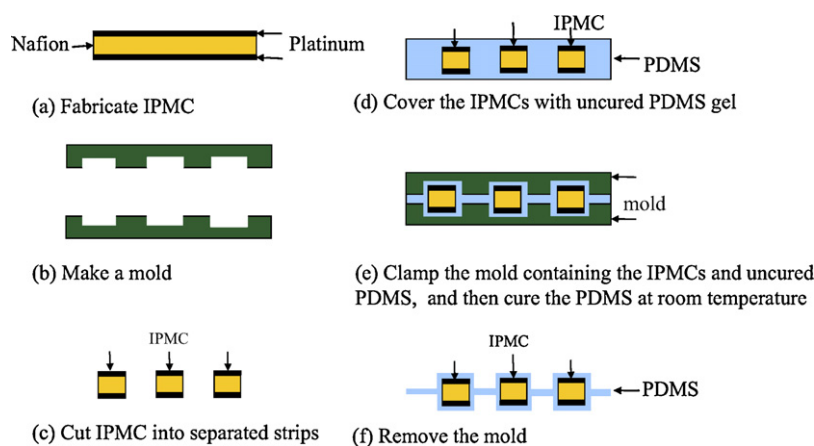


Fig. 5. Fabrication process.

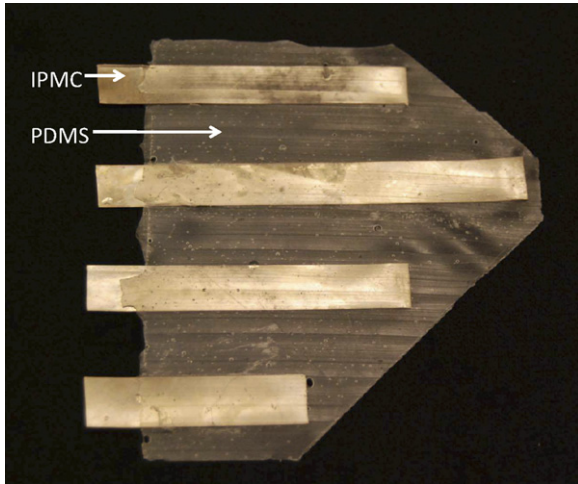


Fig. 6. IPMC/PDMS membrane actuator.

picture (cross-sectional view) of the IPMC with one platinum deposition is shown in Fig. 4(a).

Step 4 Secondary deposition. Since the surface resistance of an IPMC degrades the actuation performance [19], it is necessary to deposit more platinum metal on the surface to reduce the surface resistance. A multiple plating method has been used to deposit thicker platinum electrodes on IPMC [18]. In this study, we repeat steps 2 and 3 to grow more platinum particles on the electrodes. After the secondary deposition, the thickness of the electrode grows to $6\ \mu\text{m}$ (shown in Fig. 4(b)) and the surface resistance is reduced by 20%. Finally, the IPMC is put into a sodium ion solution to exchange the positive ions with sodium ions which are count mobile ions in the IPMC. Note that one can repeat the platinum plating process to further decrease the surface resistance. However, a thicker platinum layer also increases the stiffness of the beam, which degrades the actuation performance. The optimal thickness of the electrode is a question for future research.

2.2. PDMS molding process

The assembly process to produce an integrated IPMC/PDMS actuating membrane is shown in Fig. 5. A mold (shown in Fig. 5b) is fabricated from Delrin using a CNC rapid mill machine (MDX-650,

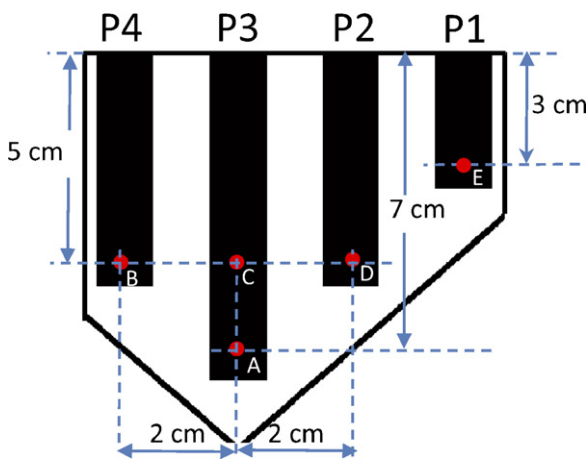


Fig. 7. Testing points of the membrane actuator.

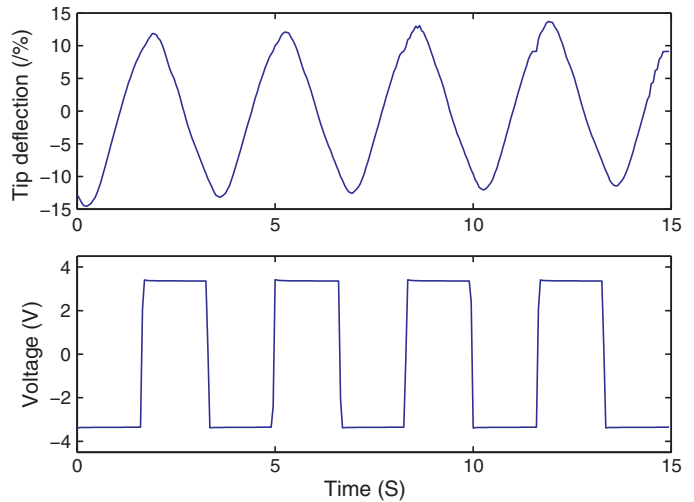


Fig. 8. Tip deflection at point A under a square wave actuation voltage (0.3 Hz, 3.3 V).

Roland). The mold is designed to house the IPMC beams ($280\ \mu\text{m}$ thick), which is then surrounded with uncured PDMS gel (Ecoflex 0030, Smooth-on Inc.). The mold, containing the IPMCs and uncured PDMS, is clamped and the PDMS is allowed to cure at room temperature for 3 h. The mold is removed leaving the IPMC/PDMS membrane actuator (Fig. 6). The PDMS has a final thickness of $190\ \mu\text{m}$ that is measured using a caliper (CD-S6^{CT}, Mitutoyo).

3. Characterization of the actuating membrane

The membrane is characterized in terms of tip deflection, tip force, twist angle, and power consumption. These characteristics are useful in providing comparison data in the design of the bio-inspired robot. To characterize the actuating response of the membrane, five testing points (A, B, C, D, E) are defined on the actuator (shown in Fig. 7).

3.1. Tip deflection measurement

The membrane is actuated in a transparent tank containing water. A laser sensor (OADM 20I6441/S14F, Baumer Electric) is fixed outside of the tank to measure the bending displacement at point A. The tip deflection is normalized by dividing the bending displacement by the length at point A. Fig. 8 shows the tip deflec-

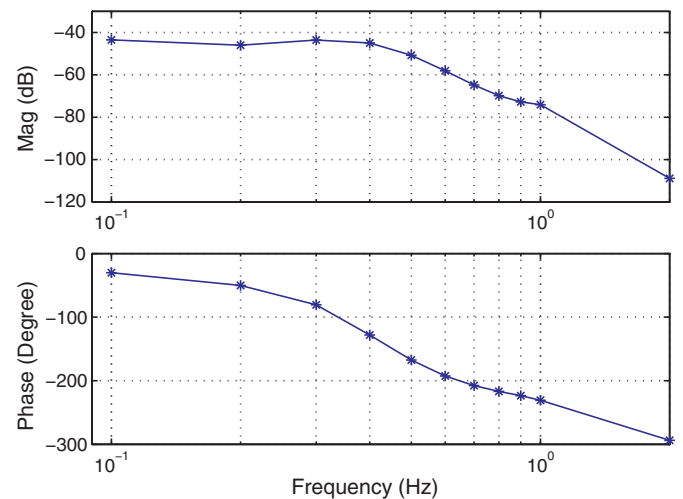


Fig. 9. Bode plot of the actuation dynamics of the membrane actuator.

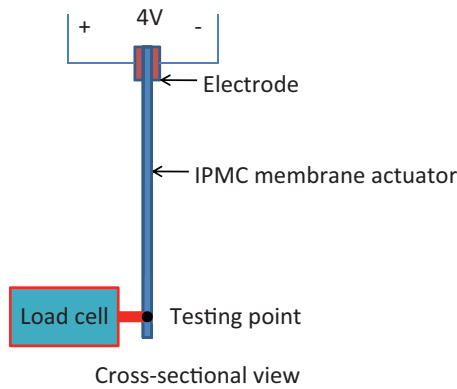


Fig. 10. Tip force measurement setup.

tion when a square wave actuation voltage (0.3 Hz, 3.3 V) is applied to all the IPMCs. It shows a peak-to-peak deflection of 25% of the spanwise dimension. One can achieve a larger deflection by applying a higher actuation voltage. There is a limit to the size of voltage applied across the IPMC – anything greater than 6 V risks dielectric breakdown through the IPMC.

To capture the Bode plot of the actuation dynamics of the actuating membrane, a series of sinusoidal actuation signals with an amplitude of 3 V and frequencies ranging from 0.1 Hz to 2 Hz are applied to the IPMCs. The bending displacement at Point A and actuation voltage are measured. The magnitude and phase shift of the displacement over the actuation voltage are calculated. The Bode plot (Fig. 9) demonstrates that the actuation dynamics of the membrane behaves as a low-pass filter with about 0.4 Hz cut-off frequency. This is to be expected as the ions in the IPMC cannot move very rapidly [20] and the hydrodynamic forces acting on the fin damp the high frequency vibration [7].

3.2. Tip force measurement

To characterize the tip force, a load cell (GS0-10, Transducer Techniques) is used to measure the tip blocking force at point A, B, D, and E (see Fig. 7). The measurement range of the load cell is from 0 to 10 g. The calibration error of the load cell, including hysteresis, nonlinearity, and non-repeatability, is 3 mg. Fig. 10

Table 1
Tip force measurement.

	At point A	At point C	At point D	At point E
\bar{F}_s (gf)	0.16	0.34	0.49	0.67
$\frac{\Delta F_s}{\bar{F}_s}$	±19%	±5.5%	±4.7%	±7.4%
T_r (S)	4.05	7.95	8.65	9.10
$\frac{\Delta T_r}{T_r}$	±1.2%	±3.1%	±1.0%	2.0%

shows the experimental setup for the tip force measurement. The measurements are taken in air and are recorded in four separate experiments. In each experiment, a 4V step voltage is applied to all the IPMCs. Fig. 11 shows the tip force response at Point A, where steady-state force F_s and rising time T_r are defined. The tip blocking force on each IPMC has been measured twice. Table 1 shows the mean values of F_s and T_s and their variations.

3.3. Power consumption measurement

For applications like an untethered bio-inspired robot, key questions regarding power consumption and how to optimally manage power consumption must be addressed. In this section, we study the power consumption under a square wave input. The power consumed by IPMCs is calculated by:

$$P = \frac{1}{T} \int_0^T i(t)v(t)dt, \quad (1)$$

where $i(t)$ and $v(t)$ are measured actuation current and voltage, respectively, and T is the period of the actuation signal. A 3.3 V and 0.22 Hz square wave voltage is applied to all the IPMCs of one actuating membrane which is fixed in a water tank. Fig. 12 shows the actuation voltage and current. To study the relation between the power consumption and frequency, a series of square wave actuation signals with an amplitude of 3.3 V and frequencies ranging from 0.22 Hz to 0.58 Hz are applied to the fin. Fig. 13 shows the power consumed versus frequency graph. It demonstrates that they are positively related and the power consumption at the cut-off frequency 0.4 Hz is 0.483 W.

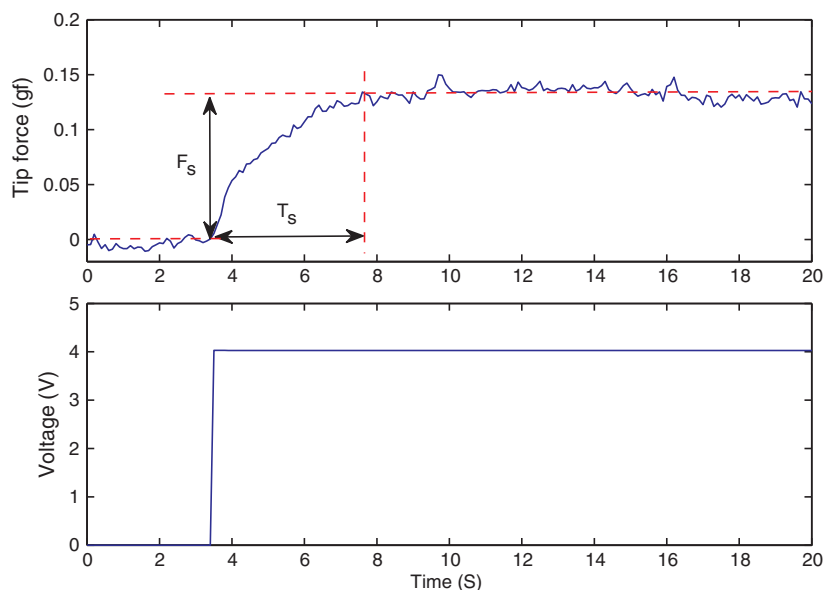


Fig. 11. Tip force measurement at point A under a 4V step actuation voltage.

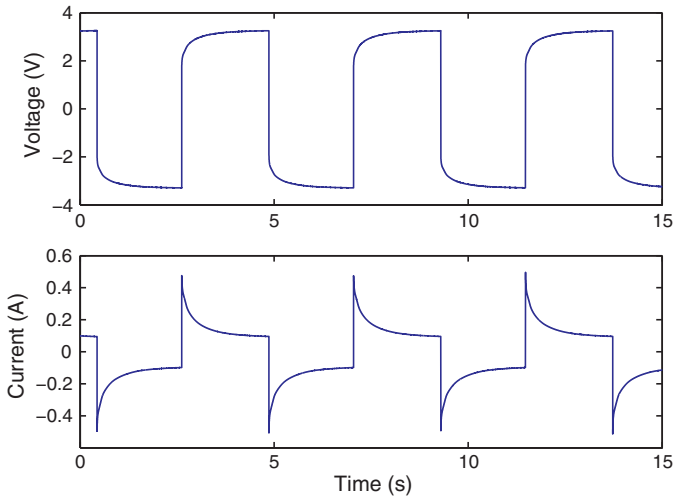


Fig. 12. Actuation current measurement.

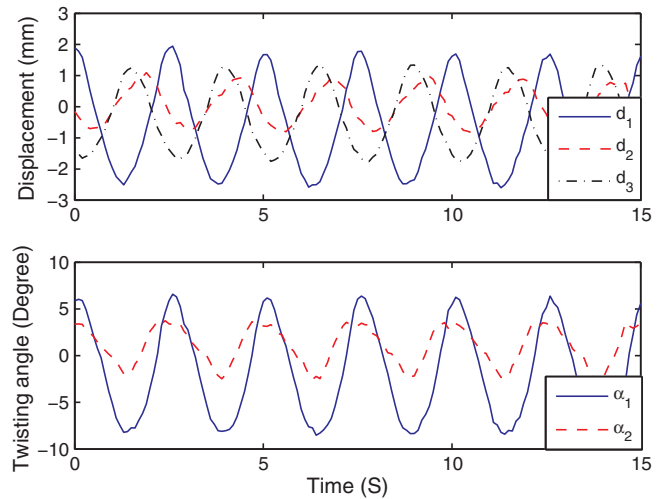


Fig. 15. Bending displacements d_1 , d_2 , d_3 , and twist angles α_1 and α_2 , under the input signals (0.4 Hz, 6 V, and 60° phase).

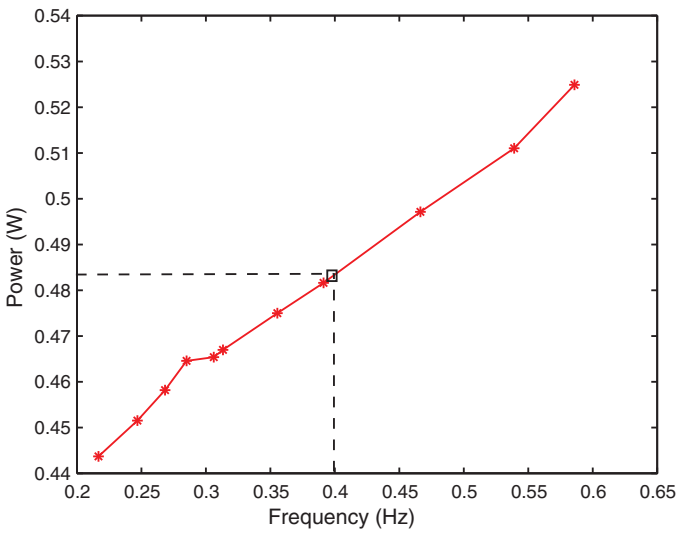


Fig. 13. Power consumption versus frequency.

calculated by

$$\alpha_1 = \arctan \frac{d_2 - d_1}{BC}, \alpha_2 = \arctan \frac{d_3 - d_2}{CD}, \quad (2)$$

where $BC = CD = 20$ mm.

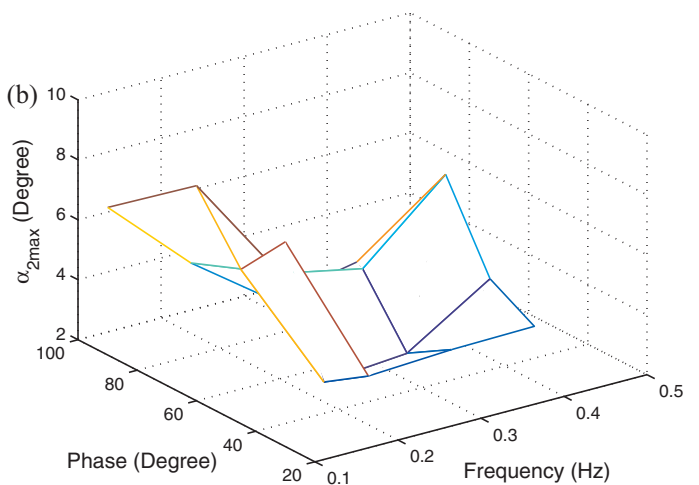
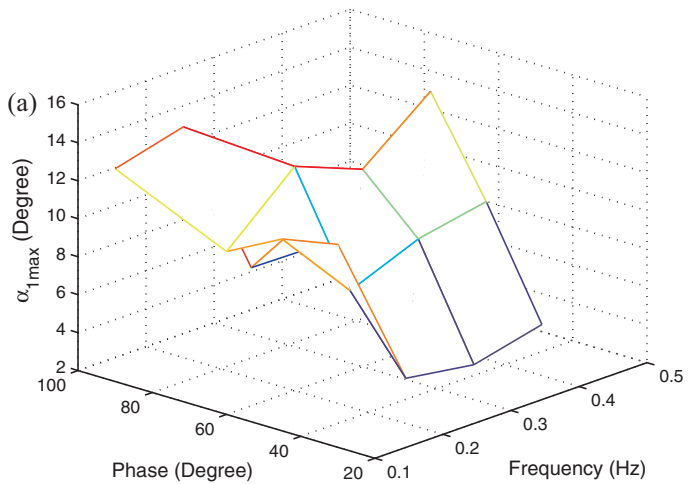
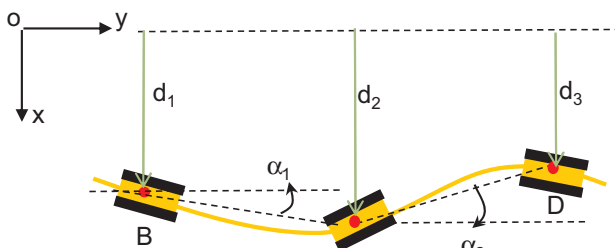


Fig. 16. Peak to peak twist angle versus different frequency and phase. (a) α_{1max} ; (b) α_{2max} .

3.4. Characterization of membrane 3D kinematics

In order to characterization of the membrane's 3D kinematics, definition of twist angle is given in Fig. 14, where points B, C, and D are defined in Fig. 7. Three laser sensors (OADM 2016441/S14F, Baumer Electric) are used to measure the bending displacements d_1 , d_2 , and d_3 at the point B, C, D, respectively. The twist angles are



Frontal cross-sectional view of the pectoral fin

Fig. 14. Definition of twist angles.

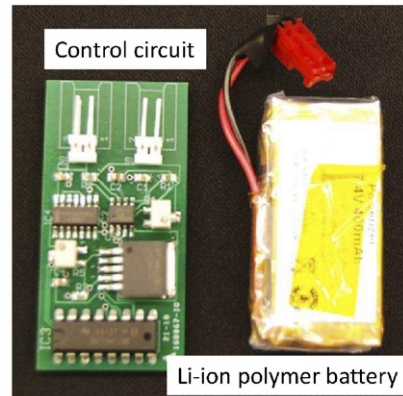
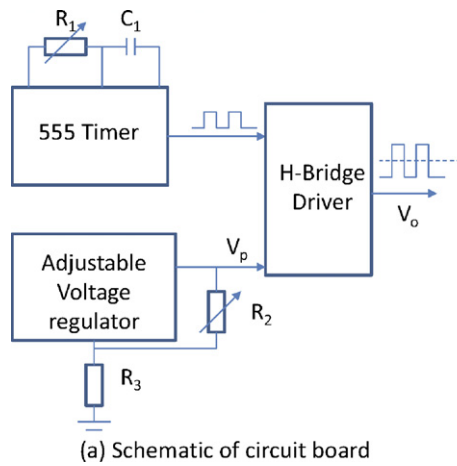


Fig. 17. On-board circuit and battery.

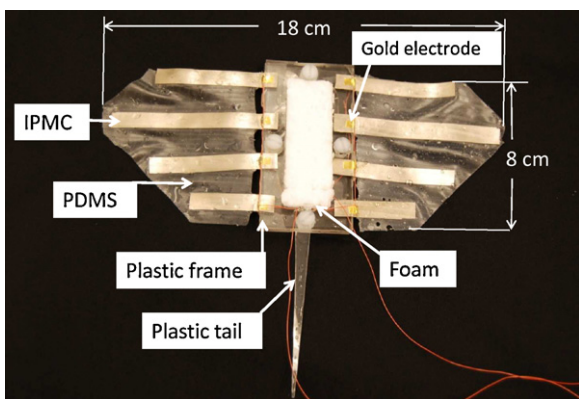


Fig. 18. A top-view picture of the robotic manta ray (without control unit).

Four sinusoidal voltage signals ($S_1, S_2, S_3,$ and S_4) are generated via Labview (National Instruments), amplified by power amplifiers, and applied to the IPMC actuators $P_1, P_2, P_3,$ and P_4 (shown in Fig. 3), respectively. All signals have the same input voltage of 6 V but varying phases. The phase ϕ in this paper is defined as the following. If $\phi = A^\circ$, then following Fig. 3, P_i leads P_{i+1} by A° , where $i = 1, 2, 3$. As mentioned earlier, IPMC actuators are used to generate thrust in underwater vehicles. Hence the kinematics are quantified in water. The actuating membrane is placed in a water tank and the laser sensors are fixed outside of the tank. Fig. 15 shows the experimental results at $\phi = 60^\circ$. The upper figure shows the bending displacement d_1, d_2 and d_3 , which clearly shows the phase delay between

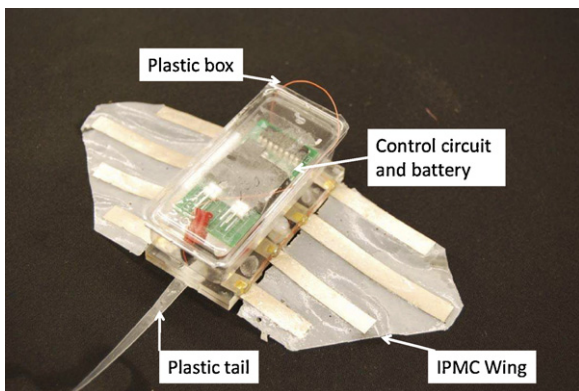


Fig. 19. A free swimming robotic manta ray with control circuits and battery.

the bending motion of the IPMC $P_1, P_2,$ and P_3 . The lower figure shows the calculated twist angles α_1 and α_2 . These results demonstrate that one can control the twist motion by manipulating ϕ . The maximum twist angle is 15.5° , which is similar to the angle generated by the pectoral fin in [13].

To demonstrate the dependence of twist angle on frequency and phase, we conducted 16 trials by changing the frequency (0.1 Hz, 0.2 Hz, 0.3 Hz, and 0.4 Hz) and phase ($30^\circ, 45^\circ, 60^\circ,$ and 90°). In each trial, the peak to peak twist angles, α_{1max} and α_{2max} , were measured. Fig. 16 shows the peak to peak twist angle versus different frequency and phase. It shows that $\alpha_1 > \alpha_2$. It may be due to the fact that the actuation of P_4 constrains the twist angle α_2 . The maximum twist angle is observed when the actuation frequency is 0.4 Hz and the phase is 60° . Because the motions of IPMCs are constrained by the soft PDMS membrane, the dynamics of the twist angle is complex.

4. Application to a robotic manta ray

To demonstrate the capabilities of this new type of actuator design, the IPMC membrane actuator is applied in the design of a bio-inspired robot. An IPMC enabled ray-like underwater robot was first developed by Anton et al, [14]. They used 16 IPMC beams connected to a latex foil to generate undulatory wave motions in the chordwise direction, which enabled rectilinear swimming in the robot. However, this design was constrained by many tethers. The actuators were controlled by a PC computer and powered by several heavy car batteries. Consequently, the robot did not demonstrate any free-swimming capability. In this paper, a small size robotic manta ray has been designed that is capable of free swimming. It includes two IPMC membrane actuator as artificial pectoral fins

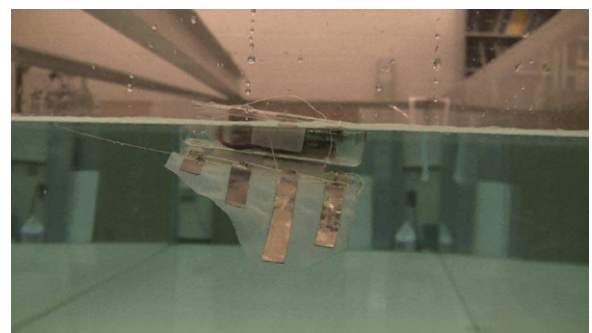


Fig. 20. A snap shot of the free-swimming robot (side view).

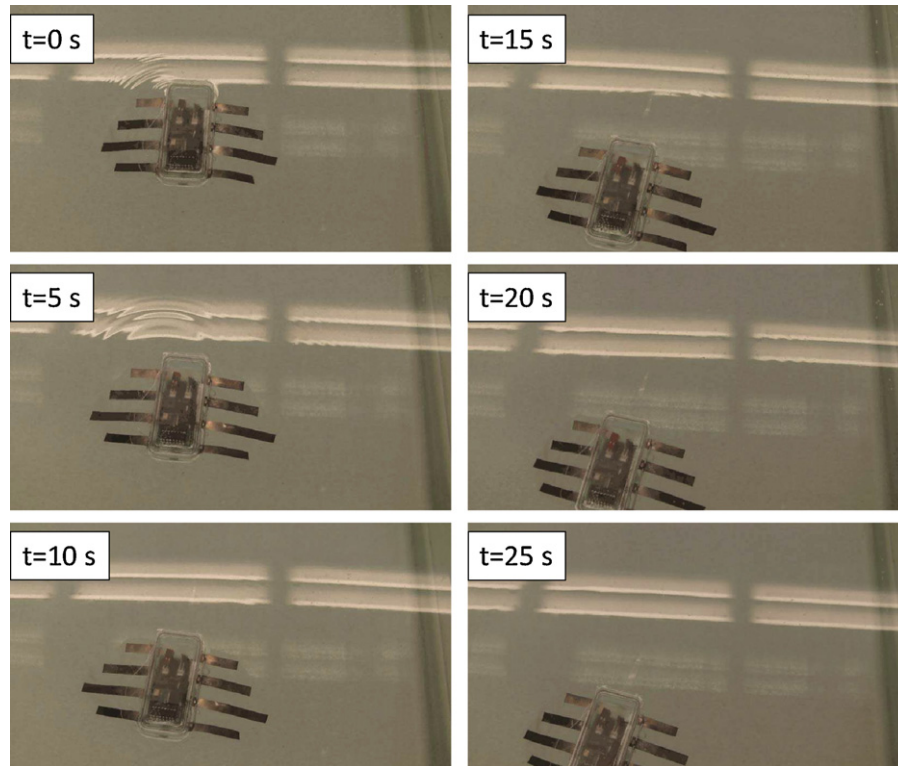


Fig. 21. Snap shots of the free-swimming robot (top view).

and a waterproof body housing an on-board control circuit and lightweight, rechargeable battery. Design of the control unit and overall robot is presented in this section.

4.1. On-board circuit and battery

The on-board circuit provides actuation voltage signals to the IPMC actuators in the wing. Fig. 17(a) shows the schematic of the circuit. In the first iteration, the circuit is able to generate one signal to all the IPMCs, generating a flapping motion. A 555 timer is used to generate a frequency tunable square wave. The amplitude of the voltage signal, V_p , is controlled by an adjustable voltage regulator. Since the 555 timer can only draw 25 mA current while the peak driving current of IPMCs in two pectoral fins is 1.5 A (shown in Fig. 12), an H-bridge driver is used to draw up to 2 A output peak current. In PCB design, most of the chips are in surface-mount package, which makes the circuit board compact (2.5 cm by 3 cm) and light (25 g).

A lithium ion battery is chosen as the power source since it is lightweight, rechargeable with high power density, and has previously been successfully implemented in IPMC actuated underwater robots [21]. A rechargeable 7.3 V lithium ion polymer battery (400 mAh, AA Portable Power Corp.) is selected for the robot. When the robot is running at 0.4 Hz, the power consumption for operating two pectoral fins is 0.96 W (shown in Fig. 13). Ideally, the robot can swim for 2.7 h without recharging when the operating frequency is 0.4 Hz. The total mass of the circuit and battery is 28.3 g. Fig. 17 (b) shows the picture of PCB board and battery.

4.2. Overall design

Fig. 18(a) shows the overall shape of the robot. Two acrylic frames with gold electrodes are made to clamp the artificial wings to the body support. Gold electrodes are used to minimize corrosion. An acrylic polymer tail is connected at the end of the robot to

aid in stabilizing the body while swimming. Polymer foam is added to make the robot neutrally buoyant. A simple hinged plastic box is used to house the circuit board and battery. Once closed, only two wires leave the box. PDMS is used to seal the housing to ensure water does not invade this compartment. The plastic box is glued on the top of the robot. When the robot is put in water, the cover of the box is above the water level and water cannot leak into the box. Design of the pectoral fins is shown in Fig. 3. The planform shape has been designed to mimic the planform shape of the pectoral fin of a batoid ray. The fully assembled robot is 8 cm long (not including the length of the tail), 18 cm wide, 2.5 cm high, and weights 55.3 g. The free-swimming robot is shown in Fig. 18 and Fig. 19.

4.3. Free swimming test

The robot is tested in a water tank (1.5 m wide, 4.7 m long, and 0.9 m deep). As the first attempt, the operating frequency of the square wave actuation voltage is tuned at 0.4 Hz and the amplitude is set at 3.3 V. A digital video camera (VIXIA HG21, Canon) is used to capture the movies of the swimming robot. Fig. 20 shows a snap shot of the free swimming robot from a side view. Fig. 21 shows six snap shots of the swimming robot from top view. Each snap shot is taken every 5 s. One can extract the speed of the robot from the movie through the Edge Detection program in the Labview. The swimming speed shown in Fig. 21 is 0.42 cm/s. Since the body length is 8 cm, one can calculate the speed is 0.053 BL/s. This is believed to be the first demonstration of an IPMC propelled free-swimming robotic batoid ray. It also validates the proposed fabrication process for making IPMC actuator capable of 3D kinematic motions.

5. Conclusions and future work

In this study, a novel synthesis technique to fabricate an IPMC membrane actuator capable of 3D kinematic motions is developed.

The actuator is fabricated by assembling IPMC actuators with a PDMS elastomer membrane. Overall the process is cost effective and less time-consuming. The actuator is characterized in terms of bending displacement, twist angle, tip force, and power consumption. The characterization results have demonstrated that the membrane actuator is capable of generating 3D kinematic motions with low power consumption. With respect to applications, a free-swimming robotic batoid ray that contains two IPMC membrane actuators as pectoral fins has been successfully built and tested. The swimming testing results show that the robot is able to swim at 0.053 BL/s with less than 1 W power consumption.

To enhance the membrane's capability of 3D kinematic motions, our future work will be focused in the following two aspects. First, we will re-design the fabrication process of IPMC to improve its actuation performance, in terms of large tip force and fast response time. Second, we will improve the stretchability of the passive area by selecting more compliant material and morphing its surface profile using microfabrication technology. To improve the speed and maneuverability of the robot, first we will develop a new on-board controller that can generate four separate channels, each with tunable amplitude and phase. The resulting system will be capable of creating undulatory motion that can generate a higher thrust force. Second, the robot body will be re-designed to mimic the body of a batoid ray, which can improve the hydrodynamics of the robot. Third, a mathematical model for the robotic manta ray will be developed to provide useful insights on how to optimize the design and control of the robot.

Acknowledgments

This research was supported in part by the Office of Naval Research (ONR) under the Multidisciplinary University Research Initiative (MURI) Grant N00014-08-1-0642 and the David and Lucille Packard Foundation.

References

- [1] Y. Bar-Cohen, Electroactive polymers as artificial muscles – capabilities, potentials and challenges, in: Y. Bar-Cohen (Ed.), *Handbook on Biomimetics*, Section 11, Chapter, 2000, pp. 1–13.
- [2] M. Shahinpoor, K. Kim, Ionic polymer–metal composites: I. fundamentals, *Smart Materials and Structures* 10 (2001) 819–833.
- [3] K.J. Kim, M. Shahinpoor, Ionic polymer–metal composites: II. manufacturing techniques, *Smart Materials and Structures* 12 (2003) 65–79.
- [4] M. Shahinpoor, Conceptual design, kinematics and dynamics of swimming robotic structures using ionic polymeric gel muscles, *Smart Materials and Structures* 1 (1) (1992) 91–94.
- [5] M. Mojarrad, M. Shahinpoor, Ion-exchange–metal composite sensor films, in: R.O. Claus (Ed.), *Smart Structures and Materials 1997: Smart Sensing, Processing, and Instrumentation*, vol. 3042, SPIE, Bellingham, WA, 1997, pp. 52–60.
- [6] S. Guo, T. Fukuda, K. Asaka, A new type of fish-like underwater microrobot, *IEEE/ASME Transactions on Mechatronics* 8 (1) (2003) 136–141.
- [7] Z. Chen, S. Sharata, X. Tan, Modeling of biomimetic robotic fish propelled by an ionic polymer metal composite caudal fin, *IEEE/ASME Transactions on Mechatronics* 15 (3) (2010) 448–459.
- [8] M. Aureli, V. Kopman, M. Porfiri, Free-locomotion of underwater vehicles actuated by ionic polymer metal composites, *IEEE/ASME Transactions on Mechatronics* 15 (4) (2010) 603–614.
- [9] L.J. Rosenberger, Pectoral fin locomotion in batoid fishes: undulation versus oscillation, *The Journal of Experimental Biology* 204 (2001) 379–394.
- [10] S. Tung, S.R. Witherspoon, L.A. Roe, A. Silano, D.P. Maynard, N. Ferraro, A MEMS-based flexible sensor and actuator system for space inflatable structures, *Smart Materials and Structures* 10 (6) (2001) 1230–1239.
- [11] P. Meissner, B.K.A.F. Riemenschneider, H. Halbritter, S. Jatta, M. Maute, M.C. Amann, Tunable long-wavelength VCSELs using a moveable mirror membrane, in: *Proceedings of the 18th Annual Meeting of the IEEE Lasers and Electro-Optics Society*, 2005, pp. 324–325.
- [12] R.O. Riddle, Y. Jung, S.-M. Kim, S. Song, B. Stolpman, K.J. Kim, K.K. Leang, Sectorized-electrode IPMC actuator for bending and twisting motion, 764221–1:9, in: *Proceedings of the SPIE Conference on Electroactive Polymer Actuators and Devices (EPAD)*, 2010.
- [13] Z. Chen, X. Tan, Monolithic fabrication of ionic polymer–metal composite actuators capable of complex deformation, *Sensors and Actuators A: Physical* 157 (2) (2010) 246–257.
- [14] M. Anton, A. Punning, A. Aabloo, M. Listak, M. Kruusmaa, Towards a biomimetic EAP robot, in: *Proceedings of Towards the Autonomous Mobile Robots*, 2004, pp. 1–7.
- [15] K.J. Kim, M. Shahinpoor, A novel method of manufacturing three-dimensional ionic polymer–metal composites (IPMCs) biomimetic sensors, actuators, and artificial muscles, *Polymer* 43 (2002) 797–802.
- [16] S.J. Kim, I.T. Lee, Y.H. Kim, Performance enhancement of IPMC actuator by plasma surface treatment, *Smart Materials and Structures* 16 (1) (2007) N6–N11.
- [17] C. Chung, P. Fung, Y. Hong, M. Ju, C. Lin, T. Wu, A novel fabrication of ionic polymer–metal composites (IPMC) actuator with silver nano-powders, *Sensors and Actuators B: Chemical* 117 (2006) 367–375.
- [18] S.J. Lee, M.J. Han, S. JunKim, J. Jho, H.Y. Lee, Y.H. Kim, A new fabrication method for IPMC actuators and application to artificial fingers, *Smart Materials and Structures* 15 (5) (2006) 1217–1224.
- [19] M. Shahinpoor, K.J. Kim, The effect of surface-electrode resistance on the performance of ionic polymer–metal composite (IPMC) artificial muscles, *Smart Materials and Structures* 9 (2000) 543–551.
- [20] S. Nemat-Nasser, J. Li, Electromechanical response of ionic polymer–metal composites, *Journal of Applied Physics* 87 (7) (2000) 3321–3331.
- [21] S. Shatara, X. Tan, E. Mbemmo, N. Gingery, S. Henneberger, Experimental investigation on underwater acoustic ranging for small robotic fish, in: *Proceedings of the 2008 IEEE International Conference on Robotics and Automation*, Pasadena, CA, 2008, pp. 712–717.